Electrochemistry Communications 115 (2020) 106719

Contents lists available at ScienceDirect

Electrochemistry Communications

journal homepage: www.elsevier.com/locate/elecom

Co–Ni nanowires supported on porous alumina as an electrocatalyst for the hydrogen evolution reaction

M. Nie[a,*], H. Sun[a], Z.D. Gao[a], Q. Li[a], Z.H. Xue[a], J. Luo[b,*], J.M. Liao[a]

[a] Chongqing Key Laboratory for Advanced Materials and Technologies of Clean Energies, School of Materials and Energy, Southwest University, Chongqing 400715, PR China

[b] Department of Chemistry, State University of New York at Binghamton, Binghamton, NY 13902, USA

ARTICLE INFO

Keywords:
Porous anodized aluminum
Alternating current electrodeposition
Hydrogen evolution reaction

ABSTRACT

Water electrolysis is a promising way to produce hydrogen fuel, but many electrocatalytic systems require electrodes made of noble metals such as platinum. There is a demand for high-efficiency, low-cost materials to replace these noble metals. Herein, porous anodic alumina (AAO) templates are prepared by direct current (DC) constant voltage anodization and the step-down method. Cobalt, nickel and Co–Ni alloy nanowires are then prepared by alternating current (AC) electrodeposition. This nanoarray system can be employed in fuel cells to minimize the use of precious metals and reduce the cost of the cathodes. The pores of the AAO template are uniform with a size range from 35 to 75 nm. Using cyclic voltammetry (CV) and linear sweep voltammetry (LSV), the Co–Ni nanowire array prepared on AAO by this method is shown to have a low overpotential for hydrogen evolution and excellent stability.

1. Introduction

Research on proton exchange membrane fuel cells (PEMFCs) has developed rapidly due to their high specific power, low working temperature and sustainability [1–5]. Noble metals such as Pt [6], Au [7] and Pd [8] are used as catalysts in PEMFCs because of their high efficiency, good reversibility and catalytic activity. Although Pt/C catalysts are widely used, they have many disadvantages, such as high cost and deactivation due to corrosion of the carbon carrier [9]. A large-scale carbon carrier also increases the thickness of the catalytic layer, influencing the speed of mass transfer and reaction [10]. Other materials used for hydrogen evolution include binary or multicomponent alloys formed by transition metals [11], such as Ni–Co and Ni–Mo, which have high electrocatalytic activity. One-dimensional structural catalysts can also improve the performance of the catalysts [12]. In this paper, the electroactive area was increased by optimizing the structure of the catalysts to improve the utilization rate and catalytic performance of the materials [13].

The template method is a common way of synthesizing one-dimensional nanomaterials [14,15], with ion-etched thin films and porous anodized aluminum oxide (AAO) thin films being the most common nanotemplates [16,17]. Porous alumina [18] is a three-layer structure composed of a porous top layer with a uniform pore diameter and tightly arranged hexagonal pores, a barrier layer with high corrosion resistance and electrical insulation, and an unoxidized aluminum substrate layer at the bottom. The technique for synthesizing Co–Ni nanowires is very mature and Co–Ni alloy is known to have good activity for the hydrogen evolution reaction, but Co–Ni nanowires supported on porous alumina have rarely been used as electrocatalysts. In this paper, porous alumina was prepared by DC constant voltage anodic oxidation [19] in oxalic acid electrolyte, and the step-down method was used in a secondary oxidation process to reduce the barrier layer without damage. The electrochemical properties of the Co and Ni nanowires and their alloys were characterized with a three-electrode system, using a Pt wire, Ag/AgCl and the AAO template with uniform pore size as the counter, reference and working electrodes, respectively.

2. Experimental section

2.1. Synthesis of the AAO template

2.1.1. Pretreatment of aluminum sheet

A high purity aluminum sheet (99.999%) was cut into pieces measuring 1 cm by 1 cm. The high purity aluminum sheet was annealed at 500 °C for 3 h in a vacuum furnace to eliminate internal stresses and other defects. The aluminum sheet was then placed in a solution of acetone and alcohol with a volume ratio of 4:1 for 10 min to remove surface oil, and then cleaned several times with deionized water. The

* Correspoding authors.
E-mail addresses: niemingcqu@126.com (M. Nie), jluo@binghamton.edu (J. Luo).

https://doi.org/10.1016/j.elecom.2020.106719
Received 12 March 2020; Received in revised form 30 March 2020; Accepted 31 March 2020
Available online 02 April 2020

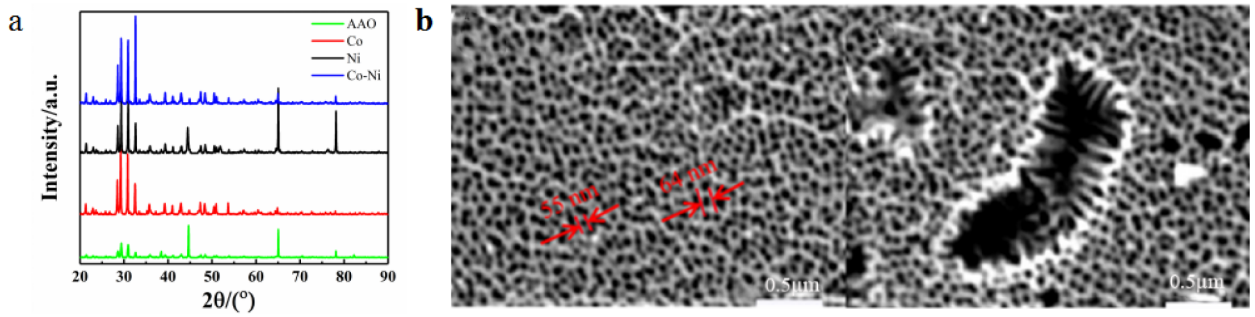

Fig. 1. (a) XRD of Ni, Co and Co–Ni alloy deposited on AAO and blank AAO; (b) SEM of the anodized aluminum template.

aluminum sheet was polished in 1 mol/L NaOH for 1 min, then rinsed several times with deionized water, and dried in a vacuum drying oven. This completed the pretreatment of the aluminum sheet.

2.1.2. Synthesis of AAO

Porous alumina templates were obtained by one- and two-step anodizations. The dry aluminum sheet described above was used as the anode, a platinum sheet as the cathode, and 0.4 mol/L oxalic acid solution as the electrolyte. The first oxidation was carried out for 4 h at a constant DC voltage of 40 V. Secondary oxidation was then carried out using the step-down method. The concentration of the electrolyte was the same as in the first oxidation. The starting voltage was set at 40 V and the voltage was reduced by 2 V every five minutes; when the voltage had reached 20 V, the voltage was reduced by 1 V every two minutes; and the reaction was stopped when the voltage reached 10 V. After the constant piezoelectric deposition had continued for 10 min, the piece of aluminum was taken out, rinsed with deionized water, and vacuum dried.

2.2. Preparation of Co, Ni and Co–Ni alloy nanowires

The porous alumina template was removed from the vacuum and an electrochemical workstation (CHI 760E, Shanghai Chenhua Instrument Company, China) was used for alternating current (AC) deposition in a three-electrode system. The solution used to electrodeposit cobalt–nickel alloy nanowires was composed of $CoSO_4{\cdot}7H_2O$ (150 g/L), $NiSO_4{\cdot}6H_2O$ (150 g/L), H_3BO_3 (30 g/L) and NaCl (6 g/L), while cobalt nanowires and nickel nanowires were electrodeposited from solutions of $CoSO_4{\cdot}7H_2O$ (150 g/L), H_3BO_3 (30 g/L), NaCl (6 g/L) and $NiSO_4{\cdot}6H_2O$ (150 g/L), H_3BO_3 (30 g/L), NaCl (6 g/L), respectively. The pH values of the three solutions outlined above ranged from 5.5 to 6.5 and could be adjusted by adding ascorbic acid. In the three electrodeposition systems studied, the AAO template was used as the working electrode, while the counter electrode and the reference electrode were a platinum wire and Ag/AgCl, respectively. Cyclic voltammetry (CV) was used to electrodeposit the metal and alloy nanowires, with a scan speed of 50 mV/s and a voltage range of 0.6 to 1.6 V. Cyclic voltammograms of the first cycle, the 500th cycle and 1000th cycle were recorded for each material.

2.3. Composition and structure characterization

X-ray diffraction (XRD, 7000S/L type, Rigaku Co, Japan) was used to analyze the phase and structure of the materials. The light source was Cu target K_α (λ = 1.5418 Å), the tube voltage 40 kV, the tube current 30 mA, and the scanning speed 5°/min. The step size was 0.02°, and the 2θ values ranged from 20° to 90°. The morphology of the materials was characterized by tungsten filament scanning electron microscopy (SEM, JSM-6610).

2.4. Electrochemical measurements

Electrochemical tests were carried out in a three-electrode system at room temperature. The AAO template was used as the working electrode, while the counter electrode and reference electrode were a platinum wire and Ag/AgCl, respectively. CV images for Co, Ni and Co–Ni after 500 cycles were compared with images for the blank AAO control group. In the blank control group, CV scanning was carried out on the AAO template in an electrolyte consisting of 30 g/L H_3BO_3 and 6 g/L NaCl without Co or Ni ions (500 cycles). The nanoarrays containing deposits of Co, Ni and Co–Ni alloys were then placed in H_2SO_4 (0.025 mol/L) for linear scanning voltammetry (LSV) and study of their Tafel curves. The dynamic parameters of the Tafel curves were calculated by an iterative method.

3. Results and discussion

3.1. Physical characterization

It can be seen from the XRD diagram in Fig. 1a that multiple diffraction peaks corresponding to Co, Ni and Co–Ni alloy appeared when AC deposition is carried out on the AAO template without removing the barrier layer or aluminum substrate. All the diffraction peaks are sharp, indicating that the synthesized sample is highly crystalline, probably composed of a variety of intermetallic compounds with Al instead of pure metal or alloy nanowires. From the SEM diagram of Fig. 1b, it can be seen that the size of the AAO pores is uniform, with a pore size of about 60 nm, and a high degree of order. It can be clearly seen from a large corrosion pit on the surface of the material that the channels are deep, neatly arranged and perpendicular to the base, while the inner walls of the channels are smooth, and the diameters of the upper and lower channels are basically the same. This shows that a sample of AAO with an orderly arrangement, uniform pore size and adjustable pore depth can be prepared by DC electrolysis under appropriate conditions.

3.2. Electrochemical characterization

Fig. 2a shows CV curves for the samples containing electrodeposited Co, Ni or Co–Ni (no blank). Comparing the CV curves we can see that the area is almost zero for Ni, while after one cycle the area corresponding to Co–Ni is the largest. There is no oxidation peak or reduction peak, which shows that the AAO template has no electrochemical activity at the beginning of AC deposition. As the number of scanning cycles increases, the length of the deposited nanowires gradually increases. The cobalt, nickel and alloy nanowires show oxidation peaks, and the peak values increase continuously, indicating that the electrocatalytic activity of the nanoarrays is also increasing. However, there are almost no reduction peaks in the curves, indicating that the electrochemical reaction in the three nanoarray systems studied is an irreversible process.

It can be seen from Fig. 2b that for a given deposition time, the oxidation peak of the Co–Ni alloy nanoarray is the highest and the area

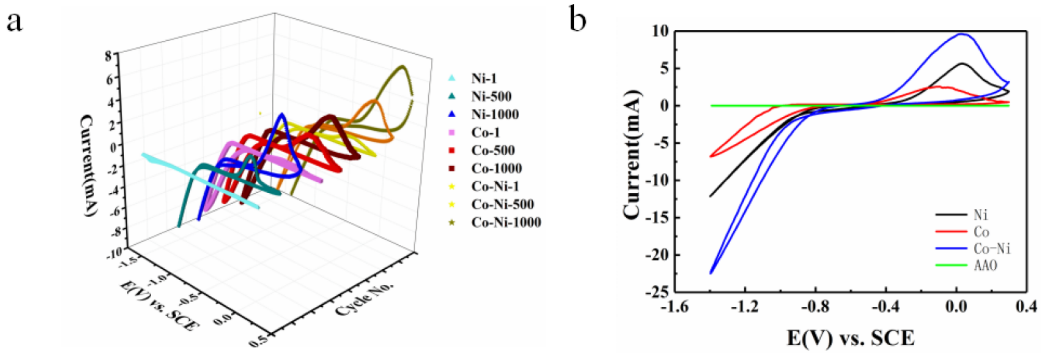

Fig. 2. (a) CV curves of the 1st, 500th and 1000th cycles of Ni, Co and Co–Ni alloys deposited on AAO (sweep rate 50 mV/s); (b) CV curves (500th cycle) of Ni, Co and Co–Ni alloy deposited on AAO and blank AAO.

of the CV image is the largest, which indicates that the electrochemical activity of the Co–Ni alloy nanoarray is the greatest. In other words, the electrochemical activity of the Co–Ni alloy nanoarray is greater than that of either the Co nanoarray or the Ni nanoarray for the same AC deposition time. In the blank control group without Co or Ni ions, the area of the CV image was almost zero, which means that no catalytic activity was shown.

Fig. 3a shows the LSV curves of AAO, Co, Ni and Co–Ni alloy. Compared with the blank AAO, the initial potentials of Co, Ni and Co–Ni alloy are shifted towards the positive direction by 0.325 V, 0.587 V and 0.694 V, respectively. The working electrodes with a Co–Ni alloy deposit show a more obvious hydrogen evolution phenomenon than an AAO template with simple metallic cobalt or nickel deposits. The results show that, compared with blank AAO, the hydrogen evolution performance of the electrode is improved when Co and Ni are deposited simultaneously.

Fig. 3b shows the Tafel curves of AAO, Co, Ni and Co–Ni alloy nanoarrays. Using the Butler-Volmer equation [20], the Tafel polarization curve was fitted to obtain the Tafel curve, and the longitudinal intercept a, the slope b and the exchange current density were calculated; the corresponding parameters are shown in Table 1. Table 1 shows that AAO with Co–Ni deposits has the largest exchange current density, which indicates the highest electrochemical activity of the electrode for hydrogen evolution. The Tafel slope for the Co–Ni alloy is found to be the highest among the electrodes studied, indicating that the transmission coefficient factor is more important [21].

Butler-Volmer equation: $j = j_0 (e^{(1-\alpha)\eta F/RT} - e^{-\alpha\eta F/RT})$.

Table 1
Tafel kinetic parameters of different electrodes in 0.025 mol/L H_2SO_4 solution.

Electrode	Tafel slope b (mV/dec)	a (V)	Exchange current density (A/cm^2)
AAO	134	0.96	1.14×10^{-10}
Co	174	0.76	1.20×10^{-5}
Ni	201	0.71	4.73×10^{-4}
Co–Ni	192	0.69	1.91×10^{-3}

4. Conclusions

In this paper, porous alumina templates with uniform pore sizes ranging from 35 nm to 75 nm were prepared by direct current electrolysis and the step-down method. Cobalt, nickel and cobalt–nickel alloy nanowires were deposited in the channels of AAO by cyclic voltammetry. The electrochemical measurements show that as the AC deposition time increases, the amount of metal deposited increases, and the electrochemical activity of the nanoarrays increases. However, there are no reduction peaks in the CV images, so the deposition process is irreversible. For a fixed number of scanning cycles, the hydrogen evolution performance of AAO loaded with Co–Ni alloy nanowire arrays is better than that of the single metal nanowire arrays. The results show that one-dimensional nanomaterials can be prepared by alternating current deposition using AAO as the template without removing the barrier layer and aluminium substrate. The metal nanoarrays also have good electrocatalytic hydrogen evolution performance and could be used in fuel cells to reduce the use of noble metals.

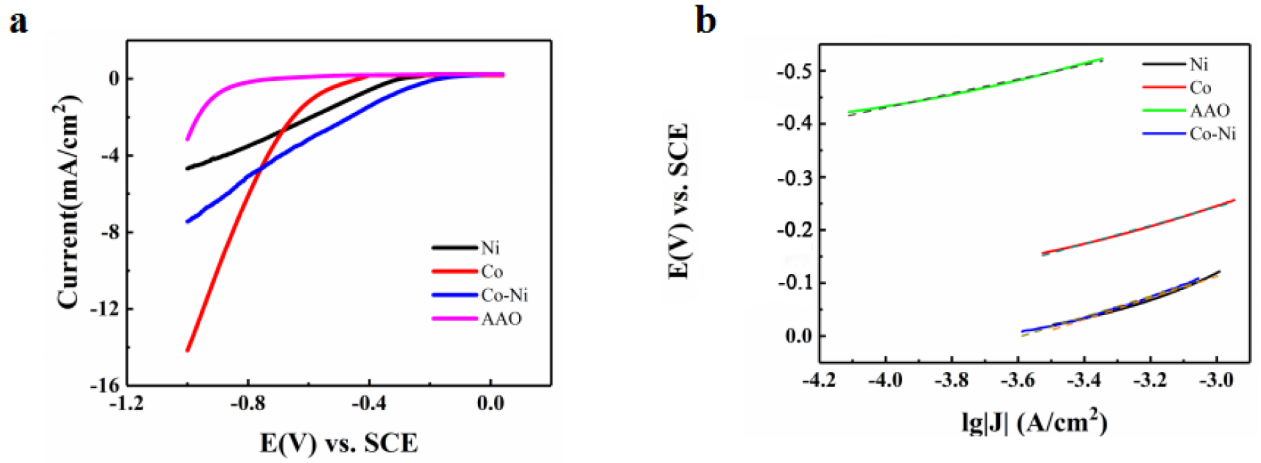

Fig. 3. (a) LSV curves of Ni, Co and Co–Ni alloys deposited on AAO compared with that of blank AAO (sweep rate 5 mV/s); (b) Tafel curves of different electrodes in 0.025 mol/L H_2SO_4 solution.

CRediT authorship contribution statement

M. Nie: Writing - review & editing. **H. Sun:** Writing - original draft, Data curation. **Z.D. Gao:** Conceptualization, Methodology. **Q. Li:** Supervision, Validation. **Z.H. Xue:** Data curation. **J. Luo:** Visualization, Investigation. **J.M. Liao:** Data curation.

Declaration of Competing Interest

The authors declare that they have no known competing financial interests or personal relationships that could have appeared to influence the work reported in this paper.

Acknowledgements

This work was supported by Fundamental Research Funds for the Central Universities (XDJK2020B004) and Chongqing Graduate Research Innovation Project (CYS19106).

References

[1] X.H. Yan, X.L. Zhou, T.S. Zhao, H.R. Jiang, L. Zeng, J. Power Sources 406 (2018) 35–41.
[2] S. Kang, L. Zhao, J. Brouwer, Renew. Energy 143 (2019) 313–327.
[3] Z. Hbilate, Y. Naimi, D. Takky, Mater. Today:. Proc. 13 (2019) 889–898.
[4] S. Gahlot, P.P. Sharma, V. Yadav, P.K. Jha, V. Kulshrestha, Colloids Surf., A 542 (2018) 8–14.
[5] M.A. Hickner, H. Ghassemi, Y.S. Kim, B.R. Einsla, J.E. McGrath, Chem. Rev. 104 (2004) 4587–4612.
[6] Y. Garsany, R.W. Atkinson, B.D. Gould, K.E. Swider-Lyons, J. Power Sources 408 (2018) 38–45.
[7] M. Beltrán-Gastélum, M.I. Salazar-Gastélum, J.R. Flores-Hernández, G.G. Botte, S. Pérez-Sicairos, T. Romero-Castañon, E. Reynoso-Soto, R.M. Félix-Navarro, Energy 181 (2019) 1225–1234.
[8] T.H. Oh, Energy 112 (2016) 679–685.
[9] S. Jing, L. Zhang, L. Luo, J. Lu, S. Yin, P.K. Shen, P. Tsiakaras, Appl. Catal. B 224 (2018) 533–540.
[10] P.J. Ferreira, G.J. la O', Y. Shao-Horn, D. Morgan, R. Makharia, S. Kocha, H.A. Gasteiger, J. Electrochem. Soc. 152 (2005) A2256.
[11] M. Zhiani, I. Mohammadi, Fuel 166 (2016) 517–525.
[12] C. Wang, H. Wang, R. Luo, C. Liu, J. Li, X. Sun, J. Shen, W. Han, L. Wang, Chem. Eng. J. 330 (2017) 262–271.
[13] C. Huff, T. Dushatinski, T.M. Abdel-Fattah, Int. J. Hydrogen Energy 42 (2017) 18985–18990.
[14] K.S. Hui, K.N. Hui, C.-L. Yin, X. Hong, Mater. Lett. 97 (2013) 154–157.
[15] K. Hnida, J. Mech, G.D. Sulka, Appl. Surf. Sci. 287 (2013) 252–256.
[16] S. Wen, S.-I. Mho, I.-H. Yeo, J. Power Sources 163 (2006) 304–308.
[17] J.S. Lee, G.H. Gu, H. Kim, K.S. Jeong, J. Bae, J.S. Suh, Chem. Mater. 13 (2001) 2387–2391.
[18] Y.-I. Park, M. Nagai, J.-D. Kim, K. Kobayashi, J. Power Sources 137 (2004) 175–182.
[19] W. Huang, M. Yu, S. Cao, L. Wu, X. Shen, Y. Song, Mater. Res. Bull. 111 (2019) 24–33.
[20] J.J. Lu, S.B. Yin, P.K. Shen, Electrochem. Energy Rev. 2 (2019) 105–127.
[21] K.K. Bera, M. Chakraborty, S.R. Chowdhury, A. Ray, S. Das, S.K. Bhattacharya, Electrochim. Acta 322 (2019) 134775.